Aleksander MAZURKOW,[1] Wojciech HOMIK[2]*

STUDIES OF SELECTED TRIBOLOGICAL CHARACTERISTICS OF SPIROID GEARS IN THE ASPECT OF MOLECULAR-MECHANICAL THEORY OF FRICTION

Summary. Spiroid gears are used in various machine drive systems in the automotive and aviation industries. They are characterised by their small size and ability to achieve high gear ratios while maintaining the positioning accuracy of the driven device. This type of gear can operate continuously or at intervals. During the operation at intervals, dry friction can occur between the mating surfaces of the face wheel teeth and the worm threads. The load, geometry and geometrical structure of the mating surfaces and the materials used determine the operation of a gear under dry friction conditions. Determining the parameters associated with dry friction provides an opportunity to develop and calculate gear characteristics, which translates into improved durability and reliability. The paper presents analyses of loads and the normal stress state in the meshing of the worm and face wheel. The authors used Hertz's theory in their study of the contact between the surfaces of the worm thread and the face wheel tooth. Static friction was analysed in the aspect of the molecular-mechanical theory of friction. The results are presented in the form of diagrams and tables describing the effect of the torque on the friction coefficient, maximum Hertzian pressures and maximum tangential stresses, as well as deformations in the contact zone between the worm and the face wheel. The results indicate that the contact stress state significantly affects selected gear performance parameters, including the friction coefficient.

1. INTRODUCTION

Spiroid gears are special-purpose gears [1-3] that are used when high gear ratios and high positioning accuracy of the driven device are required with small external dimensions [4-6]. The authors' previous study [7] confirms the possibility of using this type of gear to transmit high torque values. This is why spiroid gears are used in drive systems in, for example, the automotive and aviation industries [8-10]. Fig. 1 shows an example of a spiroid gear drive manufactured by Maxon Precision Motors Inc. for use in unmanned systems and robotics [11].

A spiroid gear has a simple construction and consists of two primary parts: a face wheel and a worm. A test bench was built to look into the operating parameters of a gear (Fig. 1). The results of the bench tests are presented in publication [12]. However, the bench tests (Fig. 1) did not provide full information on the performance characteristics, including those related to start-up, stresses and contact deformations generated in the toothed rims. Therefore, the authors decided to investigate such gear properties using numerical calculations.

---

[1] Rzeszów University of Technology; al. Powstańców Warszawy, 35-959 Rzeszów, Poland; e-mail: almaz@prz.edu.pl; orcid.org/0000-0003-1719-991X
[2] Rzeszów University of Technology; al. Powstańców Warszawy, 35-959 Rzeszów, Poland; e-mail: whomik@prz.edu.pl, orcid.org/0000-0001-7843-7761
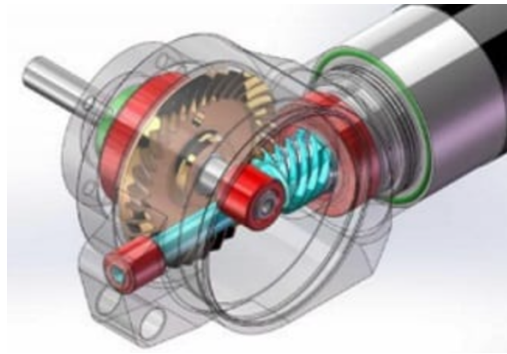* Corresponding author. E-mail: whomik@prz.edu.pl

Fig. 1. An example of a spiroid gear transmission manufactured by Maxon Precision Motors Inc. for use in
        unmanned systems and robotics [11]

Appropriate physical and mathematical models of the physical phenomena occurring during gear operation were developed to calculate the aforementioned construction characteristics. A set of parameters describing the operation of a gear was obtained by solving a system of mathematical model equations.

This article presents the results of tests on the effects of the torque transmitted by a gear on the static friction coefficient and the maximum stresses and deformations in the contact zone between the face wheel tooth and the worm thread. The test results can help determine the performance characteristics of a gear and in improving its durability and reliability.

2. ANALYSIS OF LOADS IN THE MESHING OF THE MATING WORM AND FACE WHEEL

The spiroid gear was strapped during the tests (Fig. 2). This was done to represent the actual operating conditions of a gear [13-16]. As a result of the load applied to the gear, the relation between gear output torque M_{t2} and gear input torque M_{t1} is given by:

$$M_{t1} \cdot u = M_{t2}, \quad u = \cdot \frac{\omega_1}{\omega_2}, \tag{1}$$

where: M_{t1} – gear input torque, M_{t2} – gear output torque, ω_1 – angular velocity of the worm, ω_2 – angular velocity of the face wheel, u – gear ratio.

a)   b)
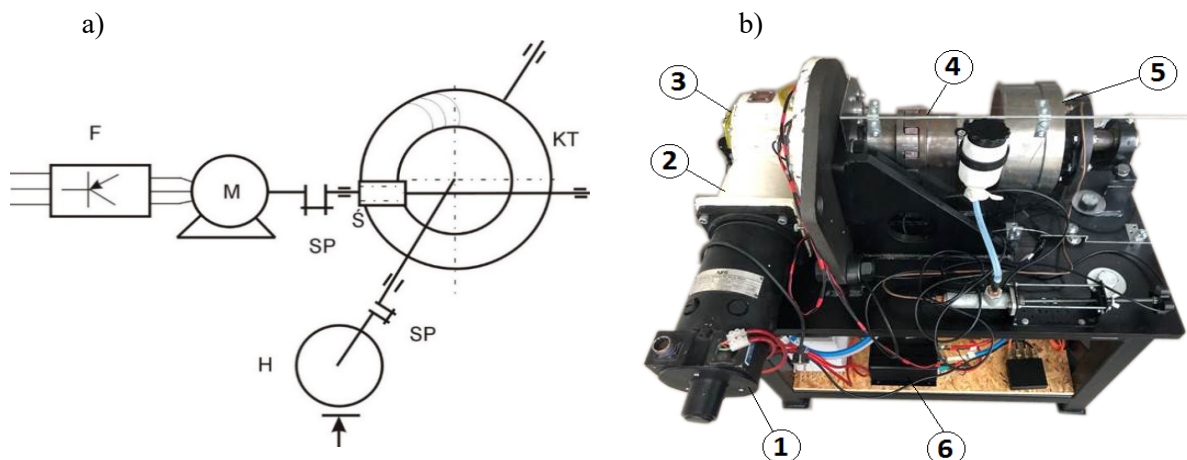

Fig. 2. Test bench: a) test bench structure: F − inverter, M − motor, SP − clutch, Ś (W) − worm, KT − face
        wheel, H − brake and b) test bench photo: 1 − motor, 2 − body, 3 − spiroid gear, 4 − clutch,
        5 − brake, 6 − measuring unit

The torque M_{t2} depends on the geometry of the toothed rim of the face wheel and the worm thread (Fig. 3) and the coefficient of static friction (f_s) between the mating surfaces.

The value of circumferential force F_{y1} depends on torque M_{t2}, which can be determined in relation to the pitch diameter of the worm using the following formula:

$$F_{y1} = \frac{M_{t2}}{r_1 \cdot u} , \tag{2}$$

where: F_{y1} – circumferential force, r_1 – pitch diameter of the worm thread.

The results of the bench tests show that the load is transmitted by four teeth of the face wheel mating with the double-thread worm. An analysis of the component forces on a single worm thread for the adopted reference system (X, Y, Z) is shown in Fig. 3. The following relations arise from this analysis:

$$F'_{y1} = F'_{ny1} + F_{ty} = F_{n1}\left(\cos\alpha_0 \cdot \sin\gamma + f'_s \cdot \cos\gamma\right) , \tag{3}$$

where: f_s– equivalent coefficient of friction given by:

$$f'_s = \frac{f_s}{\cos\alpha_0} \tag{4}$$

$$F'_{x1} = F_{n1}\left(\cos\alpha_0 \cdot \cos\gamma_1 - f'_s \cdot \sin\gamma_1\right) \tag{5}$$

$$F'_{z1} = -F_{x1} \cdot tg\alpha_0 \tag{6}$$

$$F_{t1} = F_{t2} = F'_n \cdot f_s = F_n \cdot f'_s . \tag{7}$$

The total peripheral F_{yc1} force is represented by:

$$F_{yc1} = z_k \cdot F'_{y1} , \tag{8}$$

where: z_k – the number of face wheel teeth in contact.
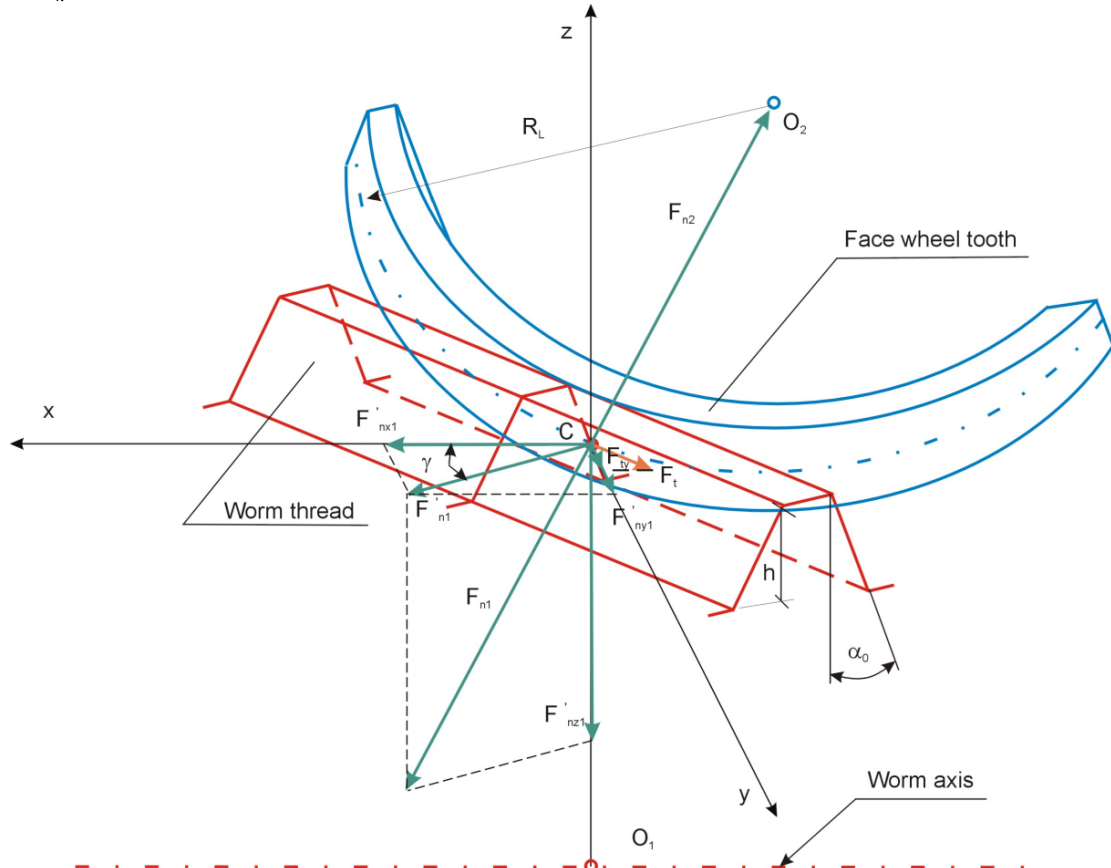

Fig. 3. Distribution of forces at the interface between the worm thread (1) and the face wheel tooth (2):
$F_n = F_{n1} = F_{n2}$ – normal force to the contact plane of the mating parts, F_t – friction force, h – tooth height, R_L – face wheel tooth line radius, α_o – tooth profile angle, γ – worm thread slope angle

3. NORMAL STRESS STATE IN THE CONTACT ZONE BETWEEN THE WORK THREADS AND THE FACE WHEEL TEETH

The analysis of contact between a flat-profile worm thread and a cylinder with radius R_L (Fig. 2) was based on the Hertzian model [17]. For the analysed gear, the contact surface between the tooth of the face wheel and the worm thread under load $F_n=F_{n1}=F_{n2}$ is a rectangle (Fig. 4) with a width of 2a and a length of b. The normal stress distribution is elliptic function $\sigma(x)$. In the Cartesian coordinate system *XY*, this function takes the following form:

$$\sigma(x) = \frac{\sigma_{H\,max}}{a}\sqrt{a^2 - x^2}, \quad -a \leq x \leq a, \tag{9}$$

where: σ_{Hmax} – Hertzian stresses, a – width of the contact surface; in angular coordinates (Fig. 3), assuming that $\varphi = arcsin\left(\dfrac{x}{R_L}\right)$, the relation is given by:

$$\sigma(\varphi) = \sigma_{H\,max}\sqrt{1 - \frac{\sin^2 \varphi}{\sin^2 \varphi_0}}, \quad 0 \leq \varphi \leq 2\varphi_0, \tag{10}$$

where: φ – angular coordinate, φ_o – contact angle derived from the centre of the contact.
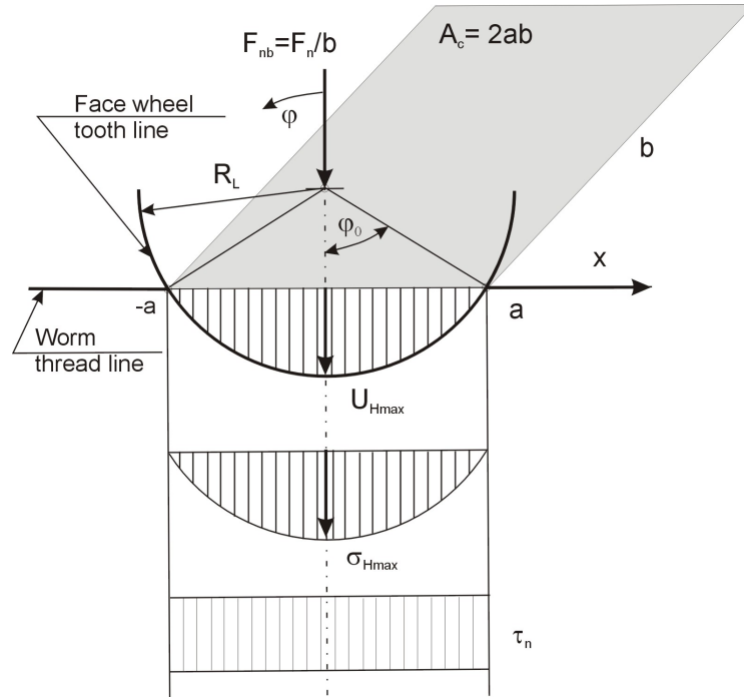

Fig. 4. Distribution of normal stresses σ_{Hmax}, tangential stresses τ_n and deformations U_{Hmax} in the contact zone between the face wheel tooth and the worm thread

The deformation of *U* points lying on the contact surface of the face wheel tooth and the worm thread is the sum of the distance *Δy*, measured before the application of the load, and the displacement *w* caused by the applied load, which can be represented by the following equation:

$$U = \Delta y + w, \tag{11}$$

where: *Δy* – the distance of the points of the face wheel profile from the work thread profile, *w* – the displacement of the contact points after the load is applied.

The solution to Equation (11) is the deformation equation, which allows the maximum deformation U_{Hmax} and the width of contact surface 2a to be determined. A detailed description of the contact phenomenon can be found in the works [17]. The deformation equation is given by:

$$E' \cdot \frac{\sigma_{H\,max} \cdot \pi}{4a} \left(2a^2 - x^2\right) = U + \rho_z \cdot x_H^2, \tag{12}$$

where: E' – equivalent Young's modulus, ρ_z – equivalent contact radius, x_H – coordinate in Hertz analysis.

The maximum displacement $U_{H\,max}$ of the contacting surfaces was determined from Equation (12) by assuming $x = 0$.

For the contact between a flat and a convex surface, equivalent Young's modulus E' and equivalent contact radius ρ_z are defined by:

$$E' = \frac{\left(1 - v_1^2\right)}{E_1} + \frac{\left(1 - v_2^2\right)}{E_2}, \quad \rho_z = \frac{1}{2 \cdot R_L}, \tag{13}$$

where: $E_{1,2}$ – Young's moduli of the worm and face wheel material, $v_{1,2}$ – Poisson's number for the material of the mating parts.

The maximum Hertzian displacement U_{Hmax} of the contacting surfaces of the face wheel tooth and the worm thread can be determined using the formula below:

$$U_{H\,max} = E' \cdot \sigma_{H\,max} \cdot \pi \cdot a, \tag{14}$$

where: $a = \sqrt{E' F_{nb} \cdot R_L}$ \hfill (15)

F_{nb} – the normal force related to the length of the contact line.

The half of the contact line a between the face wheel tooth and the worm gear used in Formula (14) and described by Relation (15) was determined assuming $x = a$, $U_{Hmax} = 0$, $b = $ const. The load related to the length of the contact line is calculated as:

$$F_{nb} = F_{nb1} = F_{nb2} = \frac{F_n}{b}, \quad b = \frac{h}{\cos\alpha_1}, \tag{16}$$

where: F_{nb1}, F_{nb2} – normal force per unit length b of contact between the worm thread and the face wheel tooth.

Consequently, the maximum normal stress in the contact zone is calculated as follows:

$$\sigma_{H\,max} = F_{nb} \cdot \frac{2}{\pi \cdot a}, \tag{17}$$

and contact angle $\varphi_0 = arcsin\dfrac{a}{R_L}$. \hfill (18)

4. TANGENTIAL STRESS STATE AND STATIC FRICTION MODEL IN THE ASPECT OF THE MECHANICAL-MOLECULAR THEORY OF FRICTION

The friction between the worm thread and the face wheel tooth during start-up was analysed using the molecular-mechanical theory of friction [18-22]. The authors assumed that the deformation of the surface layer of a solid and the intermolecular interaction at the boundary of solids are related processes. In this case, the friction force F_T is equal to the sum of the component forces, namely, molecular F_{Tm} and resistance of materials F_{Td} to deformation:

$$F_T = F_{Tm} + F_{Td} = \left(\tau_{nm} + \tau_d\right) \cdot A_r = \tau_n \cdot A_r, \tag{19}$$

where: τ_{mn} – molecular tangential stresses on the contact surface, τ_d – tangential stresses caused by the deformation of the mating gear parts, A_r – actual contact surface.

The molecular component F_{Tm} of the friction force F_T is equal to the product of the actual friction surface A_r and the tangential stresses τ_{mn} that occur on that surface:

$$F_{Tm} = A_r \cdot \tau_{nm}. \tag{20}$$

According to the molecular-mechanical theory of friction (Fig. 5), tangential stresses τ_{mn} on the friction surface depend on the shear strength of the adhesive bonds τ_o and molecular component $\beta \cdot \sigma(\varphi)$.

$$\tau_{nm} = \tau_0 + \beta \cdot \sigma(\varphi), \tag{21}$$

where: τ_o – the shear strength of adhesive bonds, β – the molecular coefficient of friction resistance, $\sigma(\varphi)$ – stress distribution.

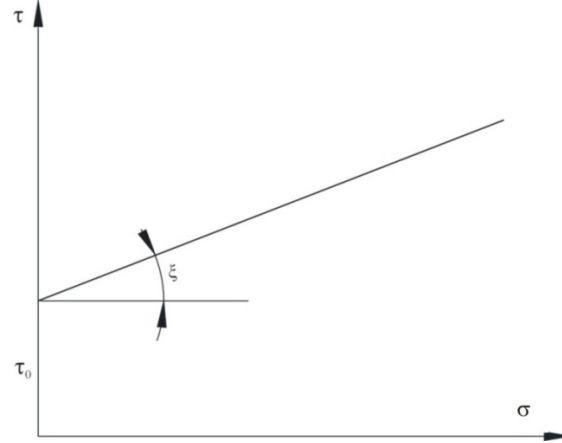Fig. 5. Dependence of tangential stresses τ as a function of normal stresses, ζ – slope angle of the flow curve of the material in the contact zone

The relation between the actual contact area A_r and the contour contact area A_c is described by the following equation:

$$A_r = \alpha \cdot A_c \cdot t_p = \alpha \cdot A_c \cdot b_\eta \cdot \varepsilon^{a_p}, \tag{22}$$

where: A_r – actual contact area, A_c – contour contact area, α – coefficient characterising the type of deformation, t_p – profile load function, a_p, b_η – coefficients of the profile load function, ε – relative depth of the penetration of the peaks of irregularities on the face wheel tooth into the worm thread. Consequently, the quotient of actual area A_r and contour area A_c is:

$$A' = \frac{A_r}{A_c} = \alpha \cdot \left[\frac{5 \cdot \sigma(\varphi) \cdot \left(1 - a_p^2\right)}{a_p \cdot \left(a_p - 1\right) \cdot k_1 \cdot E_2 \cdot \Delta^{\frac{1}{2}}} \right]^{\frac{2a_p}{2a_p+1}}, \tag{23}$$

where: k_1 – a constant whose value depends on the parameters of the profile load curve [22], Δ – dimensionless roughness index, $\Delta = \dfrac{R_{max}}{R \cdot b^{\frac{1}{v}}}$.

Assuming that the elastic deformation coefficient $\alpha = 0.5$ for elastic deformations, the molecular component of tangential stresses is given by:

$$\tau_{nm} = \frac{\tau_0}{2} \cdot \left[\frac{5 \cdot \sigma_n \cdot \left(1 - a_p^2\right)}{a_p \cdot \left(a_p - 1\right) \cdot k_1 \cdot E_2 \cdot \Delta^{\frac{1}{2}}} \right]^{\frac{2}{2 \cdot v+1}} + \beta \cdot \sigma(\varphi). \tag{24}$$

The friction force component F_{Td} depends on the deformation of the surface layer of the material of the interpenetrating surfaces of solids [22] per the following equation:

$$F_{Td} = \frac{0.25 \cdot \alpha_{ef} \cdot h_i^2 \cdot E_2}{1 - v^2}, \tag{25}$$

where: ν – Poisson's number, α_{ef} – a loss factor resulting from the influence of the hysteresis of micro-irregularity deformations [22].

The tangential stresses in the deformation zone of the micro-irregularities of the interpenetrating surfaces of solids are represented by the formula below:

$$\tau_d = \frac{F_{Td}}{A_{ri}} \cdot A',$$

(26)

where: A_{ri} – actual friction surface area related to a single micro-irregularity.

The value of A_{ri} in Equation (26) is the actual friction surface related to a single micro-irregularity (Fig. 6) and is calculated as:

$$A_{ri} = \alpha \cdot \pi \cdot R_i \cdot h_i,$$

(27)

where:
$$h_i = \left[\frac{5 \cdot \sigma(\varphi) \cdot R_i^{0,5} \cdot \left(1 - \nu^2\right) \cdot R_{max}^{\nu}}{b_p \cdot a_p \cdot \left(a_p - 1\right) \cdot k_1 \cdot E_2} \right]^{\frac{2}{2a_p + 1}},$$

(28)

R_i – radius or a micro-irregularity, h_i – deformation height, R_{max} – maximum height of the roughness profile.

By inserting Relations (27) and (28) into Equation (26), we obtain the stress component τ_d depending on the deformation of the surface layer of the face wheel material:

$$\tau_d = 0{,}0796 \cdot 0{,}5 \cdot \alpha_{ef} \cdot E_2^{\frac{-1}{2a_p + 1}} \cdot \left(1 - \nu^2\right)^{\frac{1}{a_p + 1}} \cdot \Delta^{\frac{\nu}{2a_p + 1}} \cdot \left[\frac{5 \cdot \sigma(\varphi)_n}{a_p \cdot \left(a_p - 1\right) \cdot k_1} \right]^{\frac{2a_p + 2}{2a_p + 1}}.$$

(29)

As mentioned earlier, the total tangential stresses in the actual contact area (τ_n) are the sum of the stresses arising from molecular interaction (τ_{nm}) and the stresses in the surface layer of the materials of the mating parts (τ_d).

$$\tau_n = \tau_{nm} + \tau_d = \frac{\tau_0}{2} \cdot \left[\frac{5 \cdot \sigma_n \cdot \left(1 - a_p^2\right)}{a_p \cdot \left(a_p - 1\right) \cdot k_1 \cdot E_2 \cdot \Delta^{\frac{1}{2}}} \right]^{\frac{2}{2a_p + 1}} + \beta \cdot \sigma_n +$$

$$+ 0{,}0398 \cdot \alpha_{ef} \cdot E_2^{\frac{-1}{2a_p + 1}} \cdot \left(1 - \nu^2\right)^{\frac{1}{2a_p + 1}} \cdot \Delta^{\frac{\nu}{2a_p + 1}} \cdot \left[\frac{5 \cdot \sigma(\varphi)}{a_p \cdot \left(a_p - 1\right) \cdot k_1} \right]^{\frac{2a_p + 2}{2a_p + 1}}$$
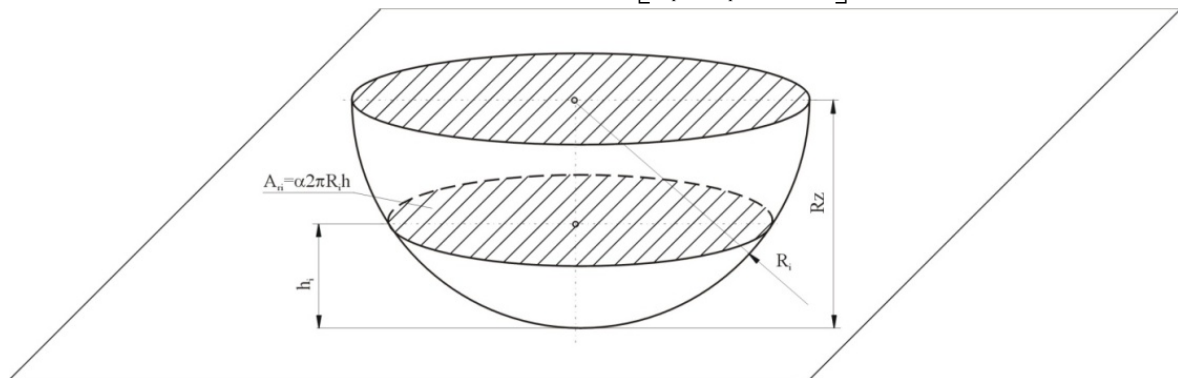
(30)

Fig. 6. Model of micro-irregularities on the face wheel tooth surface

The friction force F_{Td} from surface deformation U_{Hmax} can be treated as negligibly small compared to the molecular interaction force, assuming that the following conditions are met:

- The face wheel and the worm are made of steel with a modulus of elasticity $E_2 = 2.1 \cdot 10^{11}$ [Pa].
- The dimensionless roughness factor for an accurate surface finish is $\Delta = 1{,}1 \cdot 10^{-2}$.
- The gear can carry loads of up to $M_{tmax} = 350$ Nm.
- The profile bearing function coefficients are $a_p = b_p = 2$.

To calculate the friction force for the assumptions listed above, we used Equation (30):

$$F_t = 2 \cdot \int_0^{\varphi_0} \left[A \cdot \sigma_{H\,max}^{0,8} \cdot \left(1 - \frac{R_L^2}{a^2} \cdot sin^2 \varphi \right)^{0,4} + \beta \cdot \sigma_{H\,max} \cdot \sqrt{1 - \frac{R_L^2}{a^2} \cdot sin^2 \varphi} \right] \cdot b \cdot R_L \cdot d\varphi,$$

where: $A = \dfrac{2,16 \cdot \tau_0 \cdot \left(1 - v_2^2 \right)}{\Delta^{0,4} \cdot E_2^{0,8}}.$ \hfill (31)

Consequently, the friction torque M_{t2} on the face wheel surface is:

$$M_{t2} = f_s \cdot F_n \cdot R_L = 2 \cdot R_L^2 \cdot b \cdot \int_0^{\varphi_o} \tau_n \cdot d\varphi, \hfill (32)$$

and the coefficient of friction f_s on the actual contact surface A_r between the face wheel tooth and the worm thread, based on Equation (3), is determined using Equation (33):

$$f_s = \frac{2 \cdot R_L \cdot b \cdot \displaystyle\int_0^{\varphi_o} \tau_n \cdot d\varphi_0}{F_n}. \hfill (33)$$

5. CALCULATION OF THE OPERATING PARAMETERS OF A SPIROID GEAR

The numerical calculations were based on quantities related to the geometry of the worm and the face wheel and the materials comprising them. The gear was loaded with torques in the range of M_{t2}=35–350 Nm. The preset quantities are presented in Table 1.

For the values of torques M_{t2} used in the calculations, the distributions of normal stresses $\sigma(\varphi)$ and deformations U_{Hmax} were determined. In addition, the static friction coefficient f_s was calculated considering the mechanical and molecular properties of the materials from which the worm and face wheel were made.

The distributions of normal stresses as a function of the contact angle $\sigma(\varphi)$ and the value of torque $M_{t2} = 35, 90, 350$ Nm are presented in Fig. 7. The resultant quantities in the form of functions $\sigma_{Hmax}(M_{t2})$, $U_{Hmax}(M_{t2})$, $f_s(M_{t2})$ are presented in Figs. 8–10 and Table 2.

An analysis of the curves in the graph (Fig. 7) showed that increasing the angle φ_0 and width of contact between the face wheel and the worm thread, as well as the torque M_{t2} transmitted by the gear, increased the maximum normal stresses σ_{Hmax}. Increasing the torque M_{t2} from 35 to 950 Nm resulted in a 7.9-fold increase in stress values σ_{Hmax}.

The function $\sigma_{H\,max} = \left(M_{t2} \right)$, shown in Fig. 8, was calculated for a range of torque values $M_{t2} = 0$–1,000 Nm. As indicated by the graph of the function (and as presented earlier in Fig. 7), an increase in the value of the torque transmitted by the gear increased the maximum stress in the contact zone between the tooth of the face wheel and the worm thread. Assuming the permissible maximum value to be $\sigma_{H\,max} = 100\ MPa$ due to the operating conditions, the maximum value of the torque transmitted by the gear is $M_{t2} = 950$ Nm.

Assuming that the permissible value of deformations of the tooth surface of the face wheel equals $U_{dop} = 9.087$ μm, based on standard [23], we observed that the values of deformation were significantly lower $U_{Hmax} < U_{dop}$ in the considered load range (Fig. 9). The values of maximum deformations for the torques $M_{t2} = 35, 90, 350$ Nm are also shown in Table 2.

An analysis of Formulas (31) and (32) for calculating friction force F_t and friction torque M_t showed that static friction coefficient f_s depends on load F_n, contact surface geometry R_L, b, material properties E', β, τ_n, v and the geometric structure of the contact surface Δ. The graph of the function $f_s(M_{t2})$ shows that an increase in the value of torque M_{t2} causes a decrease in the value of friction coefficient f_s (Fig. 10). The friction coefficient f_s values for the considered torques $M_{t2} = 35, 90, 350, 950$ Nm are presented in Table 2.

Quantities used in calculations

| Geometric quantities					
Worm thread geometry			Face wheel geometry		
Number of threads	z_1	2	Number of teeth	z_2	40
Thread line lead angle	γ	5° 50'	Tooth type	Straight teeth	
Worm type	-	Left, straight teeth	Tooth height	h_2	4.4 mm
Thread height	h_1	4 mm	Tooth line	Spline	
Worm thread profile angle	α_1	30°	Tooth profile angle	α_2	30º
Inner diameter of the worm	d_{f1}	42.8 mm	Inner diameter of the face wheel	d_{w1}	117.76 mm
Outer diameter of the worm	d_{a1}	50.8 mm	Outer diameter of the face wheel	d_{z1}	152.40 mm
Type of tooth profile and tooth pitch			linear		
Radius of the face wheel tooth line			$R_L = 45.445 \cdot 10^{-3}$ m		
Gear load					
Torque on the output shaft			$M_{t2} = 35, 90, 350$ Nm		
Poisson's number			$v_1 = v_2 = 0.3$		
Young's modulus			$E_1 = E_2 = 2{,}1 \cdot 10^{11}$ Pa		
Material constants for steel 40 X					
Bearing function coefficient of the contact surface profile			$a_p = b_p = 2$		
Dimensionless roughness factor			$\Delta = 1.1 \cdot 10^{-2}$		
Coefficient of the molecular component of the friction force			$\beta = 0.055$		
Shear strength of the adhesive bonds			$\tau_0 = 184.1 \cdot 10^6$ Pa		
Material hardness			HB = 341		
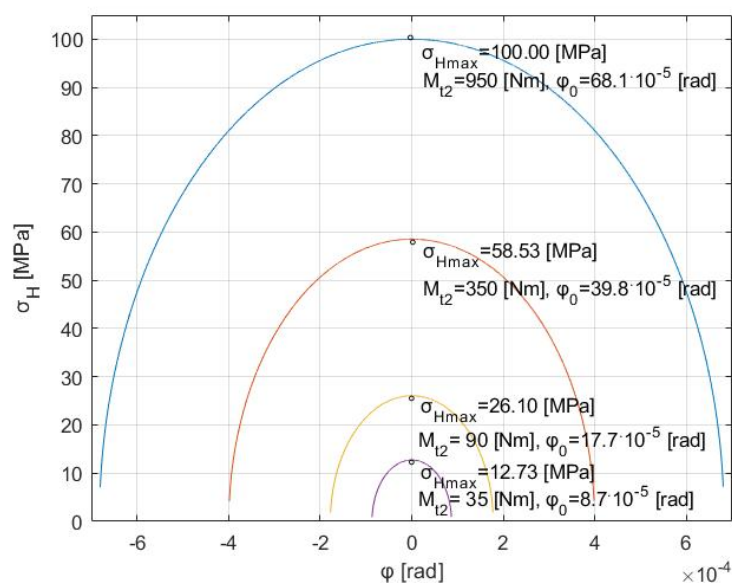
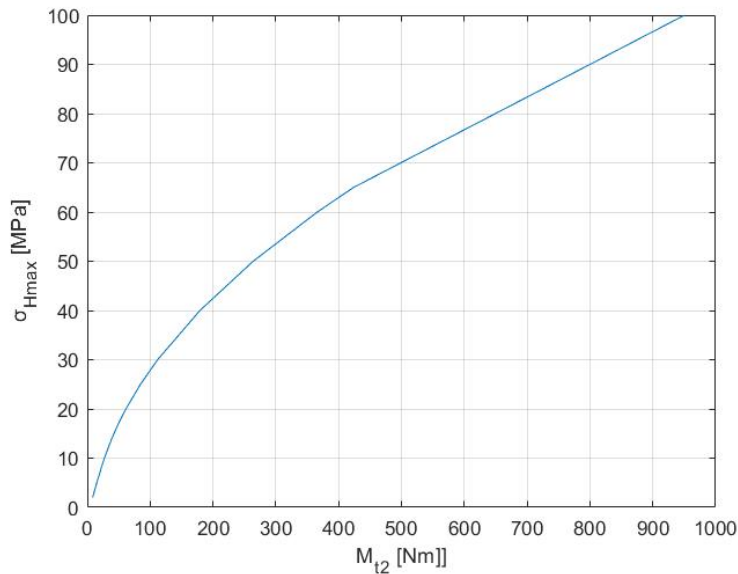Fig. 7. Normal stress distributions as a function of the face wheel and the worm thread contact angle for the Hertz model

Fig. 8. The influence of torque M_{t2} on the maximum pressures in the contact zone between the worm thread and the tooth of the face wheel σ_{Hmax}
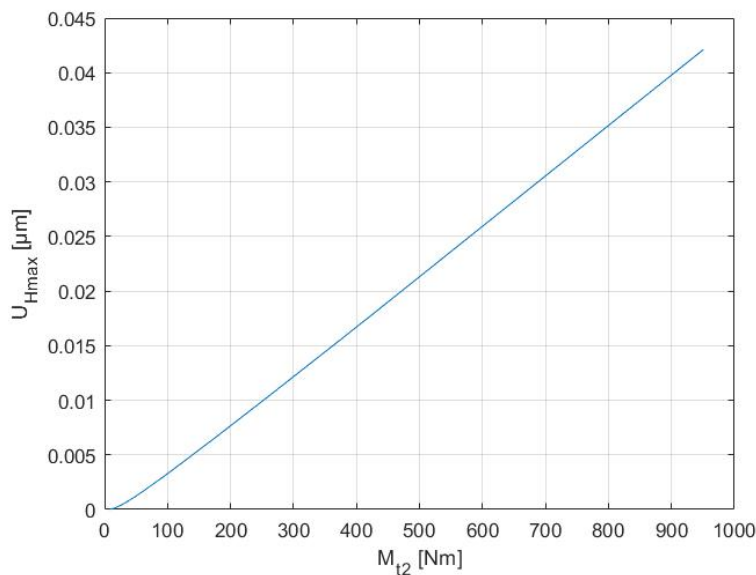

Fig. 9. The influence of torque M_{t2} on the maximum surface deformation in the contact zone between the worm thread and the face wheel tooth U_{Hmax}

6. CONCLUSIONS

Spiroid gears can operate continuously and at intervals. This paper presented test results for interval operation under dry friction conditions. Operating parameters under dry friction conditions are determined by the transferred load; the related stress state, geometry and geometric structure of the mating surfaces (worm threads and face wheel teeth); and the properties of the materials used. The results show that it is possible to evaluate gear performance based on suitably constructed characteristics. Preset and resultant parameters were assigned to build the characteristics according to the design task. The distribution of forces and stresses at the interface of the worm thread and the face wheel tooth were analysed. The influence of the torque transferred by the gear on the tangential stress state, deformation and friction coefficient was also analysed.
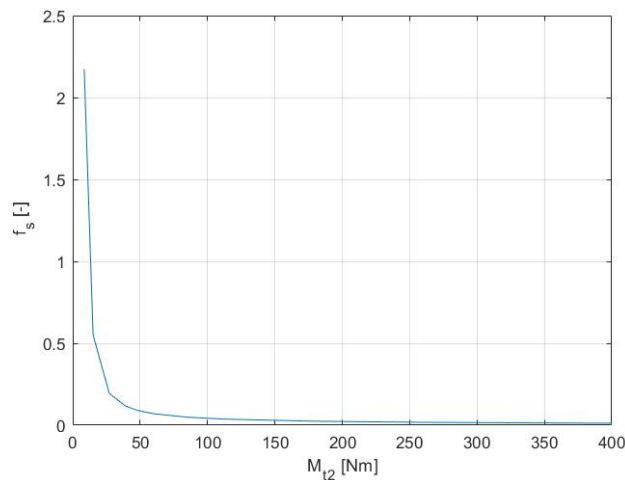
Fig. 10. The influence of gear loading torque M_{t2} on static friction coefficient f_s on the tooth surface of the face wheel mating with the worm thread

Table 2

Resultant figures

M_{t2} [Nm]	F_n [N]	F_t [N]	U_{Hmax} [μm]	φ_0[rad]	f_s [-]
35	78.4	10.7	0.0007	$8.7 \cdot 10^{-5}$	0.135
90	329.9	15.2	0.0029	$17.7 \cdot 10^{-5}$	0.046
350	1,664.8	22.8	0.0144	$39.8 \cdot 10^{-5}$	0.014
950	2,031.1	29.7	0.0421	$68.1 \cdot 10^{-5}$	0.006

The test results presented in Figs. 7–10 allowed the authors to draw the following conclusions regarding the stress state and deformations of the toothed rims and the precision with which they were made:

- Due to the maximum normal and tangential stresses and contact deformations, the gear can operate with loads $M_{t2} \leq 950$ Nm.
- Contact between the four teeth of the face wheel and two worm threads requires the bodies, the worm and the face wheel to have high manufacturing accuracy to ensure the correct positioning of the contact pattern. Otherwise, gear damage or premature wear may occur.

The test results presented in this paper extend the knowledge of mechanical and tribological properties of spiroid gears and can be helpful for gear designers. They also make it possible to increase gear durability and reliability through the appropriate selection of operating parameters. The versatility of the method presented in this paper makes it possible to determine the correct operating conditions for gears in mechanical systems used in the automotive, aviation or marine industries, along with working machines.

References

1   Goldfarb, V. & Trubachev, E. & Barmina, N. Innovations in design and production of spiroid gears in the XXI century. In: *MATEC Web of Conferences. Power transmissions.* 2019. Vol. 287. No. 01002.
2   Trubachev, E. Spiroid gears as an alternative to bevel and hypoid gears. In: *Proceedings of the 9th International Conference on Industrial Engineering (ICIE 2023).* 2023. P. 71-82.
3   Zaitsev, A. Estimation of the Resource of Spiroid Transmissions by the Condition Maximum Wear and Tear. In: Guda, A. (ed.) *Networked Control Systems for Connected and Automated Vehicles.*

Lecture Notes in Networks and Systems. Springer, Cham. 2022. Vol. 510. P. 41-49. DOI: https://doi.org/10.1007/978-3-031-11051-1_4.

4   Trubachev, E.S. & Kuznetsov, A.S. & Sannikov, A.M. *Advanced Gear Engineering*. MMS 51. Springer. 2018. P. 45-72.

5   Żabicki, D. Gear diagnostics – diagnostics, measurement, adjustment. *Chief Maintenance Officer (CMO)*, January-February 2020. [In Polish: Diagnostyka przekładni zębatych – Diagnostyka, Pomiary, Regulacja. *Główny Mechanik*. Styczeń-Luty, 2020].

6   Kazkaz, G. Mathematical modelling for the design of spiroid, helical, spiral bevel and worm. *Power transmissions.* April 2015. Available at: http://www.powertransmissions.com.

7   Mazurkow, A. Analiza obciążeń przekładni spiroidalnej. *Materiały Katedry Konstrukcji Maszyn. Politechnika Rzeszowska*. 2021. [In Polish: Analysis of spiroid gear loads. *Materials of the Mechanical Engineering Department. Rzeszów University of Technology*].

8   *Davall website*. Available at: https://www.davall.co.uk/.

9   *Spiroid website*. Available at: https://www.spiroidgearing.com/application-industries.

10   *Klingelnberg webseite.* Available at: https://www.johnhart.com.au/images/latest-news/cnc-machine-tools/Klingelnberg-GEARS-inline-2020-07.pdf.

11   Rees, C. *Maxon Precision Motors Introduces Right Angle Spiroid Gearheads.* 2015. Available at: https://www.unmannedsystemstechnology.com/2015/02/maxon-precision-motors-introduces-right-angle-spiroid-gearheads/

12   Chodoła, Ł. & Mazurkow, A. & Surowaniec, M. & Markowski, T. & Homik, W. Measurement method of temperature of the face gear rim of a spiroid gear. *Sensor*. 2022. Vol. 22(22). No. 8860.

13   Evertz, F. & Gangireddy, M. & Mork, B. & Porter, T. & Quist, A. *2022 High torque skew axis gearing. A technical primer. Spiroid high torque skew axis gearing*. 2022. Available at: https://www.spiroidgearing.com/wp-content/uploads/2019/05/Spiroid-High-Torque-Gearing-Guide.pdf.

14   Abadjiev, V. & Abadjieva, E. On approach to the synthesis, design and manufacture of hyperboloid gear sets with face mating gears. Part 1: Basic theoretical and CAD experience. *Journal of Theoretical and Applied Mechanics.* 2016. Vol. 46. No. 2. P. 3-26.

15   Frąckowiak, P. Ślad zazębienia w płaskiej przekładni spiroidalnej. *Archiwum Technologii Maszyn i Automatyzacji.* 2009. Vol. 19. No. 4. P. 59-71. [In Polish: Mesh trace in a flat spiroid gear. *Archives of Machine Technology and Automation*].

16   Litvin, F.L. & Nava, A. & Fan, Q. & Fuentes, A. New geometry of worm face gear drives with conical and cylindrical worms: generation, simulation of meshing, and stress analysis. *NASA/CR-2002-211895 ARL-CR-0511 U.S. Army Research Laboratory.* University of Illinois at Chicago, Chicago, Illinois November 2002.

17   Paluch, M. *Podstawy teorii sprężystości i plastyczności z przykładami.* Politechnika Krakowska. Kraków 2006. [In Polish: *Fundamentals of elasticity and plasticity theory with examples*. Cracow University of Technology. Cracow].

18   Bowden, F.P. & Tabor, D. *The friction and lubrication of solid.* Oxford University Press. 2023. Available at: https://academic.oup.com/book/54811.

19   Seireg, S. *Friction and Lubrication in Mechanical Design.* Taylor & Frances Ltd. 2019. Available at: https://www.scribd.com/doc/62977306/Friction-and-Lubrication-in-Mechanical-Design.

20   Goryacheva, I.G. & Dobychin, M.N. Some results concerning the development of the molecular – mechanical theory of friction. *Journal of Friction and Wear.* 2008. Vol. 29. No. 4. P. 243-250. Available at: https://link.springer.com/content/pdf/10.3103/S1068366608040016.pdf.

21   Shiping, H. & Xiao, C. & Mingqiang, X. Study on friction behavior of fractal rough surface based on molecular dynamics – Green's function method. *Chinese Journal of Theoretical and applied Mechanics*. 2023. Vol. 55. No. 7. P. 1485-1492.

22   Крагельский, И. & Михин, Н. *Узлы трения машин*. Машиностроение. Москва. 1984. [In Russian: *Friction nodes of machines*. Mechanical Engineering. Moscow].

23   ISO76:2006. *Rolling bearings – Static load ratings.* International Organization for Standardization.